Journal of Science and Technology – Smart Systems and Devices
Volume 36, Issue 2, May 2026, 120–127

Development of Multi-Stage Data Consistency Integrated U-Net Model for Undersampled MRI *k*-Space Reconstruction

Hoa Bui Thi[1], Tuyen Trong Nguyen[1], Khanh Duc Pham[1], Duc-Tan Tran[2], Anh Quang Tran[1,*]

[1]Faculty of Control Engineering, Le Quy Don Technical University, Ha Noi, Vietnam
[2]Faculty of Electrical and Electronic Engineering, Phenikaa University, Ha Noi, Vietnam
[*] Corresponding author email: anhquang.tran@lqdtu.edu.vn

Abstract

Reducing magnetic resonance imaging (MRI) acquisition time is critical to minimize patient discomfort, motion artifacts, and overall scanning costs. Compressed sensing (CS) has been widely investigated as a promising solution for MRI acceleration by reconstructing images from undersampled k-space data. However, traditional CS-based methods often suffer from instability, long reconstruction times, and limited performance due to their reliance on handcrafted regularization and iterative optimization schemes. Recent advances in deep learning have opened new possibilities for improving MRI reconstruction by learning data-driven priors directly from large datasets. Nevertheless, purely data-driven models may generate visually plausible images that lack strict consistency with the acquired measurements, potentially compromising diagnostic reliability. To address this limitation, we propose a deep learning-based MRI reconstruction framework that explicitly incorporates a data consistency (DC) layer. This physics-guided constraint enforces agreement between the network-updated k-space and the originally sampled measurements, thereby enhancing reconstruction fidelity. Experimental results demonstrate that the proposed model achieves a noticeable improvement in structural similarity index measure (SSIM) and peak signal-to-noise ratio (PSNR) compared with conventional reconstruction methods. These findings highlight the effectiveness of integrating learned priors with physics-based constraints, paving the way for faster MRI acquisition while preserving high diagnostic image quality in clinical practice.

Keywords: Compressed sensing MRI, data consistency, MRI reconstruction, U-net, undersampling *k*-space.

1. Introduction

Magnetic Resonance Imaging (MRI) is widely recognized as one of the most powerful non-invasive medical imaging techniques due to its capability to produce high-resolution images with superior soft-tissue contrast. These characteristics make MRI an essential tool for the diagnosis and evaluation of numerous medical conditions. Nevertheless, a fundamental drawback of MRI systems is the relatively long acquisition time required to collect sufficient *k*-space data for image reconstruction [1]. In clinical settings, patients are typically required to remain still for extended periods, normally varying from 40 to 60 minutes [2]. Such time-consuming scan may lead to patient discomfort, anxiety, and increased susceptibility to motion artifacts, which can significantly degrade image quality. Therefore, reducing MRI acquisition time while maintaining high diagnostic image quality has become an important and challenging research objective.

Numerous strategies have been recently proposed to accelerate MRI acquisition. These include hardware improvements [3], parallel imaging techniques [4], optimized pulse sequence design [5], and undersampling strategies in *k*-space [6, 7]. Among these approaches, compressed sensing MRI (CS-MRI) has attracted significant attention because it enables accurate image reconstruction from highly undersampled *k*-space data by exploiting sparsity in suitable transform domains. Since the pioneering works of Candès and Tao on compressed sensing theory [8], CS has been successfully applied to MRI reconstruction. In particular, Lustig *et al.* [9] demonstrated that random undersampling combined with sparsity- constrained optimization can reconstruct high-quality MRI images from substantially fewer measurements than required by the Nyquist sampling theorem [9, 10]. Subsequent studies further validated the effectiveness of CS-based MRI reconstruction using various optimization algorithms and sparsifying transforms.

However, conventional CS-MRI reconstruction methods still face several important limitations. Most CS

p-ISSN 3093-3285
e-ISSN 3093-3315
https://doi.org/10.51316/jst.190.ssad.2026.36.2.13
Received: Feb 28, 2026; Revised: Mar 23, 2026;
Accepted: Apr 5, 2026; Online: Apr 20, 2026

approaches rely on handcrafted sparsifying transforms and iterative optimization algorithms such as Nonlinear Conjugate Gradient (NCG) [10] or Orthogonal Matching Pursuit (OMP) [11]. These algorithms often involve heavy computational cost and require careful parameter tuning to achieve stable performance. Moreover, their reconstruction quality can be sensitive to sampling patterns and anatomical variations, which limits their robustness in practical clinical applications. In addition, although random undersampling theoretically satisfies compressed sensing requirements, it may lead to unstable reconstruction performance in real MRI acquisition scenarios.

Recent advances in deep learning have opened new opportunities for improving MRI reconstruction [12-14]. Deep convolutional neural networks (CNNs), particularly encoder–decoder architectures such as U-net, have demonstrated strong capability in learning complex nonlinear mappings from undersampled measurements to fully reconstructed images [15]. Several studies have shown that deep learning-based reconstruction methods can significantly outperform traditional CS-based approaches in terms of both reconstruction quality and computational efficiency [16, 17]. However, many among these purely data-driven models neglect the physical acquisition process of MRI and do not explicitly enforce consistency with the measured *k*-space data [18, 19]. As a result, these models may generate visually plausible reconstructions that contain hallucinated structures or lose important diagnostic details, which raises concerns about their reliability in clinical practice. The introduction of a data consistency (DC) as a physics-guided constraint will enforce agreement between the reconstructed image and the originally acquired *k*-space samples [20, 21]. The DC mechanism operates by selectively preserving the measured *k*-space values while allowing the network to estimate only the missing components. In this way, DC acts as a bridge between data-driven learning and the underlying physical acquisition model, effectively constraining the solution space of the reconstruction problem.

Motivated by these considerations, in this work, we propose a deep learning-based MRI reconstruction framework that integrates data consistency constraints into a cascaded U-net architecture. Our proposed approach combines the powerful representation learning capability of deep neural networks with the robustness of physics-guided reconstruction models. In particular, a DC layer is incorporated after each reconstruction stage to ensure that the reconstructed *k*-space remains consistent with the originally acquired measurements. This design will allow the proposed model to effectively balance learned image priors and physical measurement constraints.

2. Data and Methods

2.1. Dataset and Processing

In this study, experiments were conducted on publicly available brain MRI datasets, including data from the IXI database [22]. This dataset comprising nearly 600 magnetic resonance images acquired from normal, healthy subjects was employed in this study. The dataset, along with associated demographic information, was collected as part of the Information eXtraction from Images (IXI) project and is publicly available for download. The distributed archive files include multiple imaging modalities, namely T1-weighted, T2-weighted, proton density (PD), magnetic resonance angiography (MRA), and diffusion tensor imaging (DTI) scans with 15 diffusion-encoding directions.

For this investigation, a sub-dataset consisting of T1-weighted brain MRI images is selected from multiple subjects with resized images of 256×256 pixels. Consequently, a fully sampled k-space data was retrospectively undersampled using a predefined hybrid undersampling mask proposed from our previous studies [23, 24]. This under-sampling method had been also optimized as described in our recent work [25]. Particularly, this undersampling mask is designed to be applied to the full sampling *k*-space by a hybrid undersampling pattern with random/Nyquist ratio of 60/40 and a 4x acceleration factor. This 4x acceleration factor is selected as a representative and widely adopted setting in CS-MRI to ensure a fair comparison with our previous works. The undersampled *k*-space data were then reconstructed using the zero-filling or zero- padding (Z P) inverse Fourier transform, which served as the baseline input for the deep learning models [26]. The T1-weighted dataset was then partitioned into 78,110 images for training and 8,684 images for testing to ensure a reliable and unbiased evaluation of the model performance. Prior to training, data normalization along with standard preprocessing procedures was applied to the dataset. Prior to network training, all MRI slices were normalized to the intensity range [0,1] to ensure numerical stability and consistent convergence behavior. The preprocessing pipeline consists of the following steps:

1. Extraction of 2D slices from 3D MRI volumes.
2. Intensity normalization.
3. Forward Fourier transforms to obtain fully sampled *k*-space data.
4. Application of undersampling masks to simulate accelerated acquisition.
5. ZP reconstruction for baseline comparison.

These standardized preprocessing steps ensure fair comparison across different reconstruction methods

while closely mimicking realistic MRI acquisition conditions.

2.2. Undersampling and Zero-Padding Reconstruction

Let X denote the fully sampled MRI image and F is the Fourier transform (F operator). The k-space measurements Y can be expressed as (1):

$$Y=\mathrm{M}\odot\mathrm{F}(X) \quad (1)$$

where M is a binary undersampling mask and $\odot$ denotes element-wise multiplication. The ZP reconstruction [26] (X_{ZP} image) is obtained by applying the inverse Fourier transform (IFT or F^{-1}) to the undersampled k-space data is defined by this (2):

$$X_{ZP}=\mathrm{F}^{-1}(\mathrm{M}\odot\mathrm{F}(X)) \quad (2)$$

Although computationally simple, this approach results in severe aliasing artifacts and loss of fine details.

2.3. The Basic U-Net Architecture

The backbone of the proposed framework is based on a cascaded U-net architecture as shown in Fig. 1. Each U-net follows a standard encoder–decoder design with skip connections. Here, the skip-connection is used as a shortcut that allows information to travel a "short path" through one or more layers. The primary goal is to improve gradient propagation for more stable training of deep networks. The U-net, based on skip-connection, was proposed for image segmentation and subsequently widely applied in the medical field, including image reconstruction [15]. In the encoder, each level typically consists of two 3 x 3 convolutions with normalization and activation (Normalization + Activate Function), then the spatial size is reduced using max-pool or average-pooling; as you go down, the number of channels gradually increases (16→32→64→128→256…), allowing the feature learning model to become deeper and more generalizable, enabling effective multi-scale feature extraction. The encoder progressively increases the number of feature channels from 16 to 256, while the decoder restores spatial resolution through upsampling operations. This cascaded design allows multiple reconstruction stages to iteratively refine the reconstructed image, mimicking the behavior of unrolled optimization algorithms commonly used in compressed sensing MRI. This strategy will enable to improve reconstruction fidelity compared to single-pass networks.

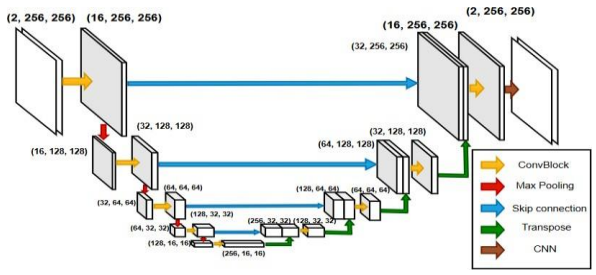

Fig. 1. The basic architecture of U-net model

Moreover, the decoder branch also increases resolution by convolutional displacements and multiplexes features from the encoder via same-level bypass connections to combine edge detail and fine texture (from the encoder) with deep feature information, allowing the network to learn the entire input data. Thanks to this mechanism, U-net is particularly suitable for medical images processing and reconstruction.

2.4 Multi-Staged U-Net Framework with DC Layer Integration

To incorporate the physical acquisition constraints of MRI into the deep learning reconstruction process, a DC layer is integrated into the proposed cascaded U-net architecture. The primary objective of this layer is to ensure that the reconstructed image remains consistent with the actually measured k-space samples obtained during the MRI acquisition process. Without this constraint, a purely data-driven network may generate visually plausible images that deviate from the true measured data, which may lead to unreliable reconstructions. Formally, X_{recon} denotes the image reconstructed by the neural network at a given stage. Its corresponding k-space representation is obtained by applying the Fourier transform F. The DC layer then enforces consistency between the reconstructed k-space and the originally acquired measurements Y. The updated k-space K_{DC} is then defined as the Equation 3:

$$K_{DC}=(1-\mathrm{M})\odot\mathrm{F}(X_{recon})+\mathrm{M}\odot\left(\frac{Y+\lambda F(X_{recon})}{1+\lambda}\right) \quad (3)$$

In this formulation, the unsampled locations ($M = 0$) are filled directly using the network-predicted k-space values. For the sampled locations ($M = 1$), the updated k-space is formulated as a weighted combination of the true measured data Y and the network prediction $F(X_{recon})$. A learnable parameter λ is explicitly introduced in this operation to control the strength of the DC constraint during training. This soft-update mechanism guarantees that the reconstruction preserves the fidelity of the measured data, while allowing the model to optimally balance between the learned image prior produced by the neural network and the originally acquired measurements. In this work, λ is initialized to 0.01 and optimized during the training process.

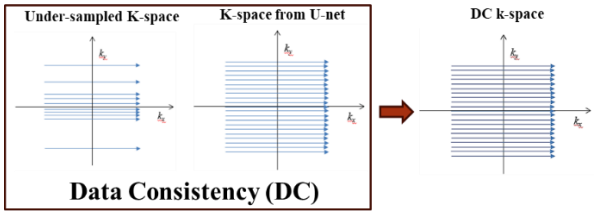

Fig. 2. The principle of DC integration

The principle of the DC operation is illustrated in Fig. 2. As shown in the figure, the reconstructed image

produced by the neural network is first transformed into *k*-space through a Fourier transform. The DC module then merges the predicted *k*-space with the originally acquired measurements using a weighted update, where a learnable parameter λ controls the balance between the two components. Specifically, the measured *k*-space samples are preserved while the missing regions are replaced by the network-estimated values. The corrected *k*-space is subsequently transformed back into the image domain using an IFT, producing an updated image that simultaneously satisfies both the learned representation and the physical measurement constraints.

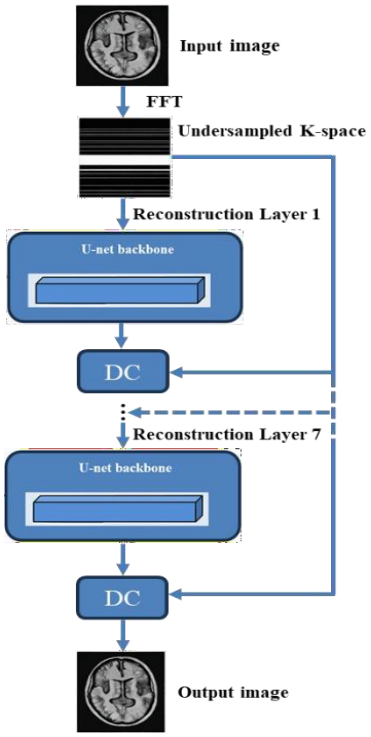

Fig. 3. The cascaded U-net framework with data consistency layer integration

To further improve reconstruction accuracy, the proposed framework adopts a cascaded architecture, as depicted in Fig. 3. Instead of performing reconstruction in a single network pass, multiple U-net modules are connected sequentially. Each stage receives the reconstructed image from the previous stage and refines it further. After each U-net reconstruction block, a DC layer is applied to enforce consistency with the measured *k*-space data before passing the result to the next stage. This cascaded design can be interpreted as an unrolled optimization process, where each stage corresponds to one refinement step of an iterative reconstruction algorithm. The U-net blocks act as learned regularization operators that suppress artifacts and recover structural details, while the DC layers enforce data fidelity. Through multiple cascaded stages, the reconstruction is progressively refined, gradually reducing aliasing artifacts and improving anatomical detail recovery. This combination provides a clear theoretical basis for the proposed architecture and explains why the cascaded model can achieve more stable and physically consistent reconstructions than a single-pass purely data-driven network.

In this study, a seven-stage cascaded U-net architecture is employed. This configuration provides a good balance between reconstruction accuracy and computational efficiency. Each stage contributes to incremental improvement of the reconstructed image, enabling the model to effectively recover high-frequency structures and suppress residual artifacts caused by undersampling.

The network is trained in a supervised manner using fully sampled MRI images as ground truth (GT). Reconstruction performance is evaluated using widely adopted quantitative metrics, including the PSNR for measuring the reconstruction fidelity by comparing the reconstructed MRI images with the fully sampled original images [27] and the SSIM [28] assess perceptual similarity between the reconstructed and reference images, which assess reconstruction fidelity and structural preservation.

3. Results and Discussions

3.1. Reconstruction Performance of the Conventional U-Net

Fig. 4 shows the number of trainable parameters in a deep learning network designed using a U-net architecture, with encoder, decoder, and upsampling layers. In the encoder branch, the convolution layers successively expand the number of feature channels from 16 → 32 → 64 → 128 → 256, thereby learning features from the local to the abstract level. The decoder branch combines the upsampling and convolution layers to restore the spatial size and concatenate with features from the encoder via a skip connection, helping to retain important details. Finally, the head layer maps to the number of output channels (in this case is 2). The total number of trainable parameters is approximately 1.94 million, indicating a moderately sized network capable of learning complex representations while remaining computationally feasible.

Layer		Shape	Params
stages.0.enc1.net.0.weight		[16, 2, 3, 3]	288
stages.0.enc1.net.3.weight		[16, 16, 3, 3]	2,304
stages.0.enc2.net.0.weight	enc2	[32, 16, 3, 3]	4,608
stages.0.enc2.net.3.weight	enc2	[32, 32, 3, 3]	9,216
stages.0.enc3.net.0.weight	enc3	[64, 32, 3, 3]	18,432
stages.0.enc3.net.3.weight	enc3	[64, 64, 3, 3]	36,864
stages.0.enc4.net.0.weight	enc4	[128, 64, 3, 3]	73,728
stages.0.enc4.net.3.weight	0.enc.4.net	[128, 128, 3, 3]	147,456
stages.0.enc5.net.0.weight	0.enc5 .net	[256, 128, 3, 3]	294,912
stages.0.enc5.net.3.weight	0.enc5 .net	[256, 256, 3, 3]	589,824
stages.0.up5.weight	0.up5.weig	[256, 128, 2, 2]	131,072
stages.0.up5.bias	0.up5.bias	[128]	128
stages.0.dec5.net.0.weight	0.dec5.net.	[128, 256, 3, 3]	294,912
stages.0.dec5.net.3.weight	0.dec5.net.	[128, 128, 3, 3]	147,456
stages.0.up4.weight	0.up4.weight	[128, 64, 2, 2]	32,768
stages.0.up4.bias	0.up4.bias	[64]	64
stages.0.dec4.net.0.weight	0.dec4.net.	[64, 128, 3, 3]	73,728
stages.0.dec4.net.3.weight	0.dec4.net.	[64, 64, 3, 3]	36,864
stages.0.up3.weight	0.up3.weight	[64, 32, 2, 2]	8,192
stages.0.up3.bias	0.up3.bias	[32]	32
stages.0.dec3.net.0.weight	0.dec3.net.	[32, 64, 3, 3]	18,432
stages.0.dec3.net.3.weight	0.dec3.net.	[32, 32, 3, 3]	9,216
stages.0.up2.weight		[32, 16, 2, 2]	2,048
stages.0.up2.bias		[16]	16
stages.0.dec2.net.0.weight		[16, 32, 3, 3]	4,608
stages.0.dec2.net.3.weight		[16, 16, 3, 3]	2,304
stages.0.head.weight		[2, 16, 1, 1]	32
stages.0.head.bias		[2]	2

Total trainable parameters: 1,939,506

Fig. 4. Trainable parameters of U-net model

The network is iterated seven stages to build a cascaded U-net network model. This proposed multi-stage model continuously improves the output through multiple stages, as each stage receiving the reconstructed image from the previous stage as input and further refining it. Therefore, this approach allows the network to gradually restore detail, reduce noise, and combine information at multiple levels. Experiments in MRI image reconstruction show that increasing the number of cascades significantly improves image quality compared to using a single network, because each stage acts as an additional optimization step. Fig. 5 shows the model's loss function, with the orange line representing the test set and the blue line representing the training set. This shows that the test set is not significantly different from the training set, indicating that the model does not fall into the category of overfitting.

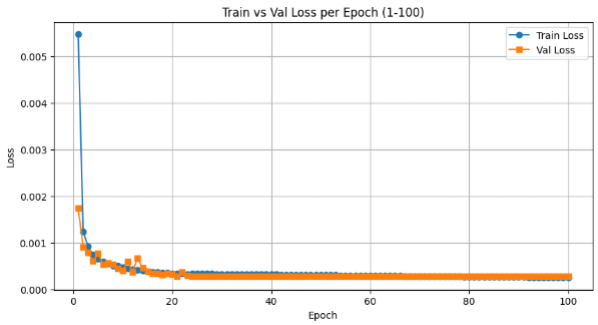

Fig. 5. The training loss function

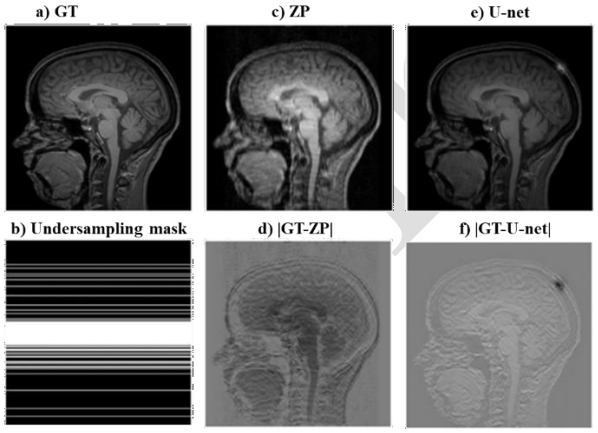

Fig. 6. The reconstructed image by the traditional U-net

To use this cascaded U-net model, the reconstruction performance of the proposed framework was comprehensively evaluated on the IXI dataset under an acceleration factor of 4X using two widely adopted quantitative metrics, PSNR and SSIM. Fig. 6 illustrates the reconstruction result obtained using the conventional U-net model. The original image or ground truth image (Fig. 6 a) is converted to the fully sampled k-space and undersamped by the hybrid undersampling mask (Fig. 6 b) before being compared with the zero-padding baseline (Fig. 6c) and the U-net (Fig. 6e), which have significantly shown the improvement in the visual quality, achieving an SSIM of 0.8434 and a PSNR of 24.81 dB by the U-net reconstruction. However, noticeable residual aliasing artifacts and blurring of fine anatomical details can still be observed, especially in high-frequency regions such as cortical boundaries and tissue interfaces. Error subtractions of reconstructed images with the GT image as shown Fig. 6d and Fig. 6f further indicate that certain high-frequency components were not fully recovered.

3.2. Reconstruction Performance of the Proposed Multi-Stage DC Integrated U-Net Model

For the integration of DC into the U-net, as aforementioned, the initial lambda learning parameter is set at 0.01, and with 7 U-net iterations, 7 lambda parameters will be added to the model. The experiment parameters as shown in Fig. 7 indicates that the DC layer integration has high performance while only negligibly increasing the computational load compared to traditional U-net architectures that add parameters to the deep learning model.

Layer	Shape	Params
stages.0.enc1.net.0.weight	[16, 2, 3, 3]	288
stages.0.enc1.net.3.weight	[16, 16, 3, 3]	2,304
stages.0.enc2.net.0.weight	[32, 16, 3, 3]	4,608
stages.0.enc2.net.3.weight	[32, 32, 3, 3]	9,216
stages.0.enc3.net.0.weight	[64, 32, 3, 3]	18,432
stages.0.enc3.net.3.weight	[64, 64, 3, 3]	36,864
stages.0.enc4.net.0.weight	[128, 64, 3, 3]	73,728
stages.0.enc4.net.3.weight	[128, 128, 3, 3]	147,456
stages.0.enc5.net.0.weight	0.enc5 .net [256, 128, 3, 3]	294,912
stages.0.enc5.net.3.weight	0.enc5 .net [256, 256, 3, 3]	589,824
stages.0.up5.weight	0.up5.weig [256, 128, 2, 2]	131,072
stages.0.up5.bias	0.up5.bias [128]	128
stages.0.dec5.net.0.weight	0.dec5.net. [128, 256, 3, 3]	294,912
stages.0.dec5.net.3.weight	0.dec5. [128, 128, 3, 3]	147,456
stages.0.up4.weight	0.up4. [128, 64, 2, 2]	32,768
stages.0.up4.bias	[64]	64
stages.0.dec4.net.0.weight	[64, 128, 3, 3]	73,728
stages.0.dec4.net.3.weight	[64, 64, 3, 3]	36,864
stages.0.up3.weight	[64, 32, 2, 2]	8,192
stages.0.up3.bias	[32]	32
stages.0.dec3.net.0.weight	[32, 64, 3, 3]	18,432
stages.0.dec3.net.3.weight	[32, 32, 3, 3]	9,216
stages.0.up2.weight	[32, 16, 2, 2]	2,048
stages.0.up2.bias	[16]	16
stages.0.dec2.net.0.weight	[16, 32, 3, 3]	4,608
stages.0.dec2.net.3.weight	[16, 16, 3, 3]	2,304
stages.0.head.weight	[2, 16, 1, 1]	32
stages.0.head.bias	[2]	2
lambdas.0	[]	1

Total trainable parameters: 1,939,507

Fig. 7. Trainable parameters of DC integrated U-net model

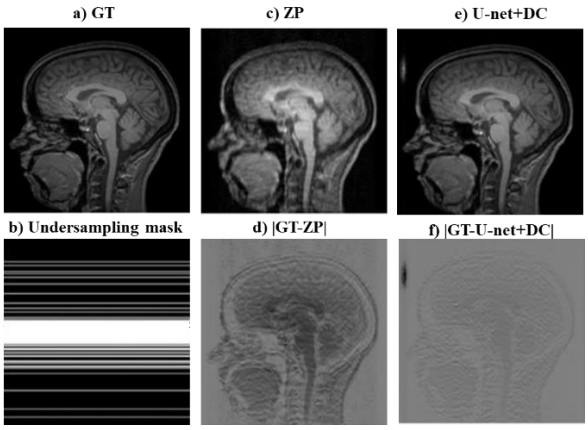

Fig. 8. The reconstructed image by the traditional DC integrated U-net network

The results described in Fig. 8 show that with just one additional learning parameter in the DC layer, the model performance has increased significantly compared to the performance of the pure U-net model. This demonstrates that the DC layer has high performance while not significantly increasing the computational load compared to other architectures that add parameters to the deep learning model.

As seen in Table 1, the ZP reconstruction yields the poorest performance due to severe aliasing artifacts, while the conventional U-net significantly improves both PSNR and SSIM by learning effective image priors from undersampled data. By integrating the DC layer into the U-net architecture, the reconstruction quality was further enhanced. The DC-augmented model achieved highest quality metrics with an SSIM of approximately 0.92, a noticeable improvement in PSNR of 29.83 and reduced reconstruction errors. Visual inspection shows sharper edges, improved contrast, and fewer artifacts compared to the conventional U-net. Notably, the inclusion of the DC layer introduces only a small number of additional learnable parameters, resulting in minimal increase in computational complexity. Nevertheless, the performance gain is significant, highlighting the effectiveness of enforcing physical consistency within deep learning-based MRI reconstruction.

Table 1. Comparison between U-net+DC and conventional methods

Reconstruction method	PSNR	SSIM
ZP IFT	19.31	0.6233
Basic U-net	24.81	0.8434
Proposed DC integrated U-net	**29.83**	**0.9162**

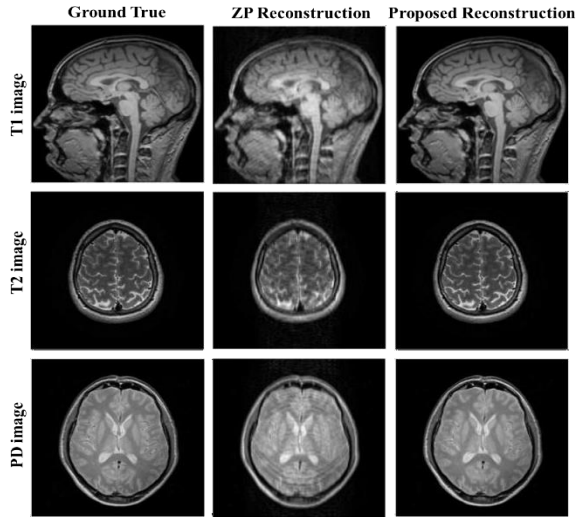

Fig. 9. Test proposed model on different T1, T2, and PD image datasets (left column is the ground truth image, middle is the ZP reconstructed image, and right is the reconstructed image from the proposed model

In addition to T1-weighted images, the proposed model was also validated on T2-weighted and Proton Density (PD) images, as illustrated in Fig. 9. The results show that, while ZP reconstruction suffers from severe noise amplification and structured aliasing artifacts, the proposed model consistently produces high-quality reconstructions with clear anatomical fidelity across different MRI modalities.

This demonstrates the strong generalization capability and robustness of the proposed framework to different tissue contrasts and imaging characteristics. From these findings, both quantitative metrics and visual comparisons consistently confirm that the proposed integration of learnable DC leads to substantial and stable improvements in undersampled MRI reconstruction quality.

3.3. Comparison between Proposed Method and Other Relevant Work

From the obtained results, it can be affirmed that while conventional deep learning models are capable of learning effective priors for MRI reconstruction, incorporating DC constraints is crucial for achieving stable and reliable performance. The proposed multi-stage U-Net with DC layers can be interpreted as an unrolled optimization process, where each stage performs a refinement step guided by both learned features and measured data. For more comprehensive evaluation of our proposed reconstruction model, we also compare the performance of our model with some other recent methods with different architectural variants-based U-net or CNN networks as described in Table 2.

Table 2. Comparison between the proposed method and other recent relevant work.

Reconstruction method	PSNR	SSIM
U-net -Dssim [29]	28.83	0.8848
Projection-based cascaded U-net[17]	33.685	0.816
Projection-based cascaded CNN [30]	32.827	0.801
BT-U-net (Transformer at Bottleneck)[31]	29.87	0.7102
Our proposed U-net+DC	**29.83**	**0.9162**

As indicated in the table, the proposed DC U-net model achieves a notable improvement over the traditional U-net, with PSNR increasing from 24.81 dB to 29.83 dB and SSIM improving from 0.8434 to 0.9162. These results demonstrate that incorporating DC substantially enhances reconstruction quality. The DC layer enforces fidelity to the acquired *k*-space measurements, ensuring physical consistency and stable reconstruction, leading to improved recovery of fine anatomical details. In the Table 2, we also compared

with other advanced architectures [29], including projection-based cascaded networks [17, 30] and transformer-based models [31], the proposed method exhibits a more balanced trade-off between PSNR and SSIM. Although some methods achieve higher PSNR values, their lower SSIM scores indicate weaker structural preservation. In contrast, the proposed model consistently maintains high structural similarity while achieving competitive reconstruction fidelity, which is particularly important for preserving diagnostically relevant features.

Moreover, although this study focuses on single-coil reconstruction, the proposed framework is inherently compatible with multi-coil or parallel MRI settings. In particular, the cascaded architecture and the DC operation can be extended by incorporating coil sensitivity information and enforcing consistency across coil-wise k-space measurements, while keeping the overall reconstruction pipeline largely unchanged. This is clinically relevant because modern MRI systems routinely employ multi-coil arrays, and our previous work has already investigated hybrid sensing strategies in parallel MRI [23]. Therefore, this study will be considered as a controlled single-coil validation of the DC-integrated architecture, with multi-coil extension being a natural and feasible next step.

Another important consideration is dataset diversity. Although the IXI dataset used in this study provides standardized and high-quality benchmark data, it mainly consists of healthy subjects. Therefore, our further work will include validation on clinical datasets containing diverse pathologies such as tumors, lesions, and other abnormal findings. Such evaluation will help determine whether the proposed model preserves subtle diagnostically relevant features without oversmoothing pathology-related structures under more challenging real-world conditions.

6. Conclusion

This research presented a data consistency integrated deep learning model for reconstructing undersampled MRI k-space data. By combining a cascaded U-Net architecture with learnable data consistency constraints, the proposed method effectively leverages both data-driven learning and physics-based MRI acquisition principles. Experimental results on brain MRI datasets demonstrate significant improvements in reconstruction quality, achieving promising enhancement in PSNR and SSIM compared to traditional reconstruction methods. The proposed framework enables accelerated MRI acquisition while preserving high diagnostic image quality, addressing a critical challenge in clinical MRI practice. Future work will focus on extending the model to multi-coil and parallel MRI scenarios, evaluating performance under different undersampling patterns and acceleration factors, and validating the approach on larger and more diverse clinical datasets.

References

[1] M. C. Florkow, K. Willemsen, V. V. Mascarenhas, E. H. G. Oei, M. van Stralen, and P. R. Seevinck, Magnetic resonance imaging versus computed tomography for three-dimensional bone imaging of musculoskeletal pathologies: A review, Journal of Magnetic Resonance Imaging, vol. 56, iss. 1, pp. 11–34, Jan. 2022. https://doi.org/10.1002/jmri.28067

[2] K. G. Hollingsworth, Reducing acquisition time in clinical MRI by data undersampling and compressed sensing reconstruction, Physics in Medicine & Biology, vol. 60, no. 21, pp. R297–R322, Oct. 2015. https://doi.org/10.1088/0031-9155/60/21/R297

[3] P. Sharma, A. K. Dubey, and A. Goyal, Hardware acceleration using SIMD based vector processor array to enhance performance of deblurring methods for CT and MRI images having motion blur artifacts, in ICSSES, Tumakuru, India, Jul. 2023. https://doi.org/10.1109/ICSSES58299.2023.10199266

[4] J. Hamilton, D. Franson, and N. Seiberlich, Recent advances in parallel imaging for MRI, Progress in Nuclear Magnetic Resonance Spectroscopy, vol. 101, pp. 71–95, Aug. 2017. https://doi.org/10.1016/j.pnmrs.2017.04.002

[5] N. Corbin, S. Miraux, V. Ozenne, E. Ribot, and A. Trotier, Fast imaging and acceleration techniques, in The Challenges of MRI: Techniques and Quantitative Methods for Health, London, UK, of Wiley-ISTE, ch. 3, pp. 51–74, Apr. 2024. https://doi.org/10.1002/9781394284030.ch3

[6] S. Kojima, H. Shinohara, T. Hashimoto, and S. Suzuki, Undersampling patterns in *k*-space for compressed sensing MRI using two-dimensional Cartesian sampling, Radiological Physics and Technology, vol. 11, pp. 303–319, Aug. 2018. https://doi.org/10.1007/s12194-018-0469-y

[7] M. Sandilya, and S. R. Nirmala, Compressed sensing trends in magnetic resonance imaging, Engineering Science and Technology, an International Journal, vol. 20, iss. 4, pp. 1342–1352, Aug. 2017. https://doi.org/10.1016/j.jestch.2017.07.001

[8] E. J. Candes, J. Romberg, and T. Tao, Robust uncertainty principles: exact signal reconstruction from highly incomplete frequency information, IEEE Transactions on Information Theory, vol. 52, iss. 2, pp. 489–509, Feb. 2006. https://doi.org/10.1109/TIT.2005.862083

[9] M. Lustig, D. L. Donoho, J. M. Santos, and J. M. Pauly, Compressed sensing MRI, IEEE Signal Processing Magazine, vol. 25, iss. 2, pp. 72–82, Apr. 2008. https:// doi.org/10.1109/MSP.2007.914728

[10] M. Lustig, D. Donoho, and J. M. Pauly, Sparse MRI: The application of compressed sensing for rapid MR imaging, Magnetic Resonance in Medicine, vol. 58, iss. 6, pp. 1182–1195, Oct. 2007. https://doi.org/10.1002/mrm.21391

[11] J. A. Tropp and A. C. Gilbert, Signal recovery from random measurements via orthogonal matching pursuit, IEEE Transactions on Information Theory, vol. 53, iss. 12, pp. 4655–4666, Jan. 2008. https://doi.org/10.1109/TIT.2007.909108

[12] M. Safari, Z. Eidex, C.-W. Chang, R. L. J. Qiu, X, and X. Yang, Advancing MRI reconstruction: A systematic review of deep learning and compressed sensing integration, Biomedical Signal Processing and Control, vol. 111, Jan. 2026, Art. no. 108291. https://doi.org/10.1016/j.bspc.2025.108291

[13] R. Heckel, M. Jacob, A. Chaudhari, O. Perlman, and E. Shimron, , Deep learning for accelerated and robust MRI reconstruction, Magnetic Resonance Materials in Physics, Biology and Medicine, vol. 37, pp. 335–368, Jul. 2024. https://doi.org/10.1007/s10334-024-01173-8

[14] A. Yang, M. Finkelstein, C. Koo, and A. H. Doshi, Impact of deep learning image reconstruction methods on MRI throughput, Radiology: Artificial Intelligence, vol. 6, iss. 3, Mar. 2024. https://doi.org/10.1148/ryai.230181

[15] W. Jiangtao, N. I. R. Ruhaiyem, and F. Panpan, A comprehensive review of U-Net and its variants: advances and applications in medical image segmentation, IET Image Processing, vol. 19, iss. 1, Apr. 2025, Art. no. e70019. https://doi.org/10.1049/ipr2.70019

[16] A. M. ElBehairy, I. A. Yassine, and M. Elattar, Stage U-Net framework: Streamlining MRI reconstruction from under- sampled K-space, in EECSS'24, Barcelona, Spain, 2024. https://doi.org/10.11159/mvml24.111

[17] A. Aghabiglou and E. M. Eksioglu, Projection-based cascaded U-Net model for MR image reconstruction, Computer Methods and Programs in Biomedicine, vol. 207, Aug. 2021, Art. no. 106151. https://doi.org/10.1016/j.cmpb.2021.106151

[18] J. Huang, Y. Wu, F. Wang, Y. Fang, Y. Nan, C. Alkan, D. Abraham, C. Liao, L. Xu, Z. Gao, W. Wu, L. Zhu, Z. Chen, P. Lally, N. Bangerter, K. Setsompop, Y. guo, D. Rueckert, G. Wang, and G. Yang, Data- and physics-driven deep learning based reconstruction for fast MRI: fundamentals and methodologies, IEEE Reviews in Biomedical Engineering, vol. 18, pp. 152–171, Jan. 2025. https://doi.org/10.1109/RBME.2024.3485022

[19] K. Hammernik, T. Küstner, B. Yaman, Z. Huang, D. Rueckert, F. Knoll, and M. Akçakaya, Physics-driven deep learning for computational magnetic resonance imaging: combining physics and machine learning for improved medical imaging, IEEE Signal Process Magazine, vol. 40, iss. 1, pp. 98-114, Jan. 2024. https://doi.org/10.1109/MSP.2022.3215288

[20] M. Safari, S. Wang, Z. Eidex, R. L. J. Qiu, C.-W. Chang, D. S. Yu, and X. Yang, A Physics-informed deep learning model for MRI brain motion correction, Medical Physics, vol. 52, iss. 12, Dec. 2025, Art. no. e70197. https://doi.org/10.1002/mp.70197

[21] D. Karkalousos, S. Noteboom, H. E. Hulst, F. M. Vos, and M. W. A. Caan, Assessment of data consistency through cascades of independently recurrent inference machines for fast and robust accelerated MRI reconstruction, Physics in Medicine & Biology, vol. 67, no. 12, Art. no. 124001. https://doi.org/10.1088/1361-6560/ac6cc2

[22] brain-development.org, IXI dataset (RRID:SCR_005839), 2025.

[23] A. Q. Tran, T-A. Nguyen, P. T. Doan, D-N. Tran, and D-T. Tran, Parallel magnetic resonance imaging acceleration with a hybrid sensing approach, Mathematical Biosciences and Engineering, vol. 18, iss. 3, pp. 2288–2302, Mar. 2021. https://doi.org/10.3934/mbe.2021116

[24] A. Q. Tran, T.-A. Nguyen, V. T. Duong, Q.-H. Tran, D. N. Tran, and D.-T. Tran , MRI Simulation-based evaluation of an efficient under-sampling approach, Mathematical Biosciences and Engineering, vol. 17, iss. 4, pp. 4048–4063, Jun. 2020. https://doi.org/10.3934/mbe.2020224

[25] D. K. Pham, D -T. Tran, and A. Q. Tran, Evaluating random–Nyquist sampling ratios in combined compressed sensing magnetic resonance imaging, Bulletin of Electrical Engineering and Informatics, vol. 14, iss. 6, 2025. https://doi.org/10.11591/eei.v14i6.10333

[26] X. Zhu, B. Tomanek, and J. Sharp, A pixel is an artifact: On the necessity of zero-filling in fourier imaging. Concepts in Magnetic Resonance Part A, vol. 42A, iss. 2, pp.32–44, Feb. 2013. https://doi.org/10.1002/cmr.a.21256

[27] P. Jyoti and K. Raj, Peak signal to noise ratio analysis in single image restoration technique, International Journal Of Advance Research, Ideas And Innovations In Technology, vol. 5, iss. 4, Jan. 2019 pp. 160–162.

[28] M. Punga, S. Moldovanu, and L. Moraru, Structural similarity analysis for brain MR image quality assessment, in AIP Conference Proceedings, vol. 1634, iss. 1, pp. 137–143, Nov. 2014. https://doi.org/10.1063/1.4900418

[29] V. Ghodrati, J. Shao, M. Bydder, Z. Zhou, W. Yin, K.-L. Nguyen, Y. Yang, and P. Hu, MR image reconstruction using deep learning: evaluation of network structure and loss functions, Quantitative Imaging in Medicine and Surgery, vol. 9, no. 9, Oct. 2019. https://doi.org/10.21037/qims.2019.09.12

[30] D. Kocanaogullari and E. M. Eksioglu, Deep learning for MRI reconstruction using a novel projection based cascaded network, in 2019 IEEE MLSP, Pittsburgh, PA, USA, 2019.

[31] B. Dong and G. Wu, A swin transformer-based cold diffusion model for accelerated MRI reconstruction, in Proc. IEEE GAIIS 2025, Hangzhou, China, 2025, pp. 226–230. https://doi.org/10.1145/3728726.3728760